AGU PUBLICATIONS

JGR

Journal of Geophysical Research: Atmospheres

RESEARCH ARTICLE
10.1002/2016JD025497

Key Points:
- We compare LST and T_{air} over a 5000 m elevation range to assess if LST is a good proxy for assessing spatial and temporal variations in T_{air}
- Daytime LST/T_{air} contrasts both increase and becomes less consistent with increasing elevation, but nighttime contrasts do not
- Nighttime LST is a more reliable proxy for spatial and temporal changes in T_{air}

Correspondence to:
N. C. Pepin,
nicholas.pepin@port.ac.uk

Citation:
Pepin, N. C., E. E. Maeda, and R. Williams (2016), Use of remotely sensed land surface temperature as a proxy for air temperatures at high elevations: Findings from a 5000 m elevational transect across Kilimanjaro, *J. Geophys. Res. Atmos.*, *121*, 9998–10,015, doi:10.1002/2016JD025497.

Received 16 JUN 2016
Accepted 2 AUG 2016
Accepted article online 4 AUG 2016
Published online 5 SEP 2016

Use of remotely sensed land surface temperature as a proxy for air temperatures at high elevations: Findings from a 5000 m elevational transect across Kilimanjaro

N. C. Pepin[1], E. E. Maeda[2], and R. Williams[1]

[1]Department of Geography, University of Portsmouth, Portsmouth, UK, [2]Department of Geosciences and Geography, University of Helsinki, Helsinki, Finland

Abstract High elevations are thought to be warming more rapidly than lower elevations, but there is a lack of air temperature observations in high mountains. This study compares instantaneous values of land surface temperature (10:30/22:30 and 01:30/13:30 local solar time) as measured by Moderate Resolution Imaging Spectroradiometer MOD11A2/MYD11A2 at 1 km resolution from the Terra and Aqua platforms, respectively, with equivalent screen-level air temperatures (in the same pixel). We use a transect of 22 in situ weather stations across Kilimanjaro ranging in elevation from 990 to 5803 m, one of the biggest elevational ranges in the world. There are substantial differences between LST and T_{air}, sometimes up to 20°C. During the day/night land surface temperature tends to be higher/lower than T_{air}. LST-T_{air} differences (ΔT) show large variance, particularly during the daytime, and tend to increase with elevation, particularly on the NE slope which faces the morning Sun. Differences are larger in the dry seasons (JF and JJAS) and reduce in cloudy seasons. Healthier vegetation (as measured by normalized difference vegetation index) and increased humidity lead to reduced daytime surface heating above air temperature and lower ΔT, but these relationships weaken with elevation. At high elevations transient snow cover cools LST more than T_{air}. The predictability of ΔT therefore reduces. It will therefore be challenging to use satellite data at high elevations as a proxy for in situ air temperatures in climate change assessments, especially for daytime T_{max}. ΔT is smaller and more consistent at night, so it will be easier to use LST to monitor changes in T_{min}.

1. Introduction

There is concern that mountain areas in comparison to adjacent lowlands may show enhanced warming in response to greenhouse forcing due to factors such as snow-albedo feedback, changes in atmospheric moisture, and the laws of physics [see *Rangwala and Miller*, 2012; *Pepin et al.*, 2015]. However, surface temperature observations are skewed toward lower elevations [*Lawrimore et al.*, 2011], and the current observational network is inadequate to determine whether high elevations are warming more rapidly than lower elevations. Numerous studies have investigated observational evidence for elevation-dependent warming, but while some show an increase in warming rates in high mountains [*Diaz and Bradley*, 1997; *Ohmura*, 2012; *Yan and Liu*, 2014], others show a decrease [*Lu et al.*, 2010; *Vuille and Bradley*, 2000; *Ceppi et al.*, 2010; *You et al.*, 2010] or a more complex picture [*Pepin and Lundquist*, 2008].

Remotely sensed temperatures have the advantage of extensive spatial coverage, often at fairly high resolution [*Merchant et al.*, 2013], but so far, relatively few studies have used this potential data source in the context of temperature trends at high elevations [*Qin et al.*, 2009]. Although this is partly because of the short length of the satellite records, this is becoming less relevant with time. However, satellites measure land surface or "skin" temperature (hereafter referred to as LST) [*Jin and Dickinson*, 2010] as opposed to air temperature at screen level (~2 m above ground; hereafter referred to as T_{air}). The latter is commonly used for climate change assessments [*Hartmann et al.*, 2013] and is a critical measurement in ecology, hydrology, and climate science. LST is more strongly controlled by the surface radiation balance [*Benali et al.*, 2012], which is in turn controlled by the interplay between local land surface characteristics and solar geometry, while T_{air} tends to be more regional in scope, although rapid variations can occur over short distances due to factors such as cold-air drainage [*Daly et al.*, 2010; *Lundquist et al.*, 2008]. Thus, if satellite records are to be applied to examine elevation-dependent

warming, studies which compare LST and T_{air} at extremely high elevations (>4000 m) are required. So far, comparisons have been limited to lowland [*Coll et al*., 2009; *Vancutsem et al*., 2010] or moderate elevation environments [*Wenbin et al*., 2013; *Shamir and Georgakakos*, 2014].

This paper therefore compares Moderate Resolution Imaging Spectroradiometer (MODIS) LST from the MOD11A2/MYD11A2 products [*Wan*, 2006] with T_{air} along a transect of 22 weather stations across Kilimanjaro, including sites at elevations up to 5800 m. The elevational range of nearly 5000 m is one of the largest in the world. The main aim is to understand the contrast between LST and T_{air} and uncover the factors that control this. Previous studies are discussed in section 2. The study area is outlined and methods are explained in section 3. The main behavior of the difference between LST and T_{air} is examined in section 4, along with the factors that control its variation, before the consequences of our findings are discussed.

2. Previous Studies Comparing LST and T_{air} in Different Regions

MODIS LST is produced as a series of MOD11 (Terra) and MYD11 (Aqua) products, validated with in situ measurements in more than 50 clear-sky cases in the temperature range of 263–331 K (for details see *Wan et al*. [2002, 2004], *Wan* [2006], *Wan* [2008], *Wang et al*. [2008], and *Coll et al*. [2009]). A generalized split-window algorithm [*Wan and Dozier*, 1996] is used to retrieve LST at 1 km resolution. LST has been compared with T_{air} in a range of environments including the Arctic [*Urban et al*., 2013; *Østby et al*., 2014; *Westermann et al*., 2012], midlatitude continental areas [*Shen and Leptoukh*, 2011; *Hachem et al*., 2012; *Benali et al*., 2012; *Wenbin et al*., 2013], and the tropics [*Maeda et al*., 2011; *Vancutsem et al*., 2010]. Vegetation plays a key role on LST especially in the tropics, but snow cover and ice cover are important at higher latitudes and elevations.

Comparing LST and T_{air} at Voi in Kenya (savannah vegetation), *Maeda et al.* [2011] showed a high correspondence at night (22:30 local solar time) but significant differences during the day (10:30 local solar time). Larger differences were observed around the equinoxes when solar input was strongest. *Mostovoy et al.* [2005] also showed seasonal differences in the LST/T_{air} temperature relationship over Mississippi. Larger differences in summer were related to changes in vegetation. *Vancutsem et al.* [2010] also show that differences between daytime LST and T_{air} vary according to the ecosystem and solar radiation input at the surface. *Benali et al.* [2012] developed statistical models to predict LST from T_{air} in Portugal using variables including day length, elevation, and continentality. In high latitudes the presence of extensive snow cover reduces variability in the difference between LST and T_{air} [*Hachem et al*., 2012], but LST is consistently colder. Cloud cover could introduce systematic bias in LST [*Westermann et al*., 2012], and it is difficult to separate cloud cover and snow cover, especially when patchy, due to similarities in thermal emission. *Shamir and Georgakakos* [2014] examined contrasts between LST and T_{air} at moderate elevations in eastern Turkey in an area with seasonal snow cover. The relationship between the two was strongly dependent on snow cover. Daytime LST excesses of 15–20°C were recorded in summer when snow was absent, but daytime LST sometimes became colder than T_{air} when snow was present.

Most studies conclude that LST is much more spatially variable than T_{air}, particularly during periods of strong insolation (daytime) and when there is patchy cloud and/or snow. Such situations are common in the tropics (convective cloud) and at high elevations. The extreme radiation climate at high altitudes [*Barry*, 2008] is thus expected to increase the variability between LST and T_{air} further. Both ephemeral snow cover and vegetation contrasts (e.g., across treelines) are also expected to influence differences at high elevations. However, there have been no detailed comparisons of LST and T_{air} at elevations above 4000 m because of the paucity of reliable air temperature data.

Much of the work using satellite temperature data in Africa and in the Kilimanjaro area has concentrated on the effect of vegetation on surface temperatures [*Maeda et al*., 2011; *Maeda and Hurskainen*, 2014]. This is unsurprising given the central influence of land use change, in particular deforestation and land cover change, on tropical environmental change [*Soini*, 2005]. Rapid change has been observed on Kilimanjaro [*Shugart et al*., 2001; *Lambrechts et al*., 2002; *Hemp*, 2005; *Fairman et al*., 2011]. Vegetation density and state can be measured by the normalized difference vegetation index (NDVI) [*Townshend and Justice*, 1986] which can be obtained from the MODIS sensor reflectance measurements. The NDVI is calculated as follows:

$$\mathrm{NDVI} = \frac{(\rho_{\mathrm{NIR}} - \rho_{\mathrm{Red}})}{\rho_{\mathrm{NIR}} + \rho_{\mathrm{Red}}}$$

where ρ_{NIR} is the near-infrared reflectance and ρ_{Red} is the red reflectance. MODIS products can offer NDVI imagery with different preprocessing levels in terms of atmospheric correction, cloud screening, and bidirectional reflectance distribution function effect removal. *Maeda and Hurskainen* [2014] showed that NDVI (as measured by MOD13Q1) had a strong influence on LST patterns across Kilimanjaro during the daytime in addition to elevation, drier areas with lower NDVI having increased LST, but the strength of this effect varied seasonally. During the night this influence disappeared and elevation became the dominant control.

The negative relationship between NDVI and daytime LST has been used as the basis of the temperature/vegetation index method [*Nemani and Running*, 1989], which applies this correlation to correct LST to provide an improved estimate of T_{air}. LST becomes more similar to T_{air} when vegetation is healthy (high value of NDVI) because the canopy has an effective radiative temperature close to the air temperature. However, this method has shown limited success at high elevations on the Tibetan Plateau [*Wenbin et al*., 2013], and at extremely high elevations vegetation is absent.

The aim of this study is to understand the different climatologies of LST and T_{air} across Kilimanjaro, a location with an extreme elevation range and strong environmental gradients in moisture, vegetation, and snow cover. It is expected that LST will be more spatially and temporally variable than T_{air}, particularly during the day, and that decoupling between LST and T_{air} will increase at the highest elevations.

3. Methods

3.1. Study Area

Kilimanjaro is an isolated mountain in northern Tanzania with a summit elevation of 5895 m. The base lies below 1000 m, meaning that this is one of the largest and highest free-standing mountains in the world. The mountain covers numerous ecological zones (Figure 1) [*Hemp*, 2006a]. The lower slopes (submontane belt: 1000–1800 m) are dominated by agriculture and support a high population, mainly through coffee and banana cultivation and small-scale subsistence farming (Figure 1a) [*Hemp*, 2006b]. Above 1800 m most of the natural cloud forest has been preserved, especially on the southern slopes (Figure 1b), although the northern slopes are much drier. The cloud forest extends up to around 3000 m, above which is the giant-heather zone (~3100–3900 m; Figure 1c) dominated by *Erica arborea*. Above 3900 m the dominant vegetation becomes alpine heathland/moorland including *Helichrysum* cushion vegetation (Figure 1d). Above 4500 m there is very little vegetation and the environment is arid and dominated by the extreme radiation regime of high elevations (Figure 1e). There are small summit ice fields within the summit crater (Figure 1f).

The climate of Kilimanjaro has been extensively studied [*Coutts*, 1969; *Hastenrath*, 1991; *Hastenrath and Greischar*, 1997], most recently in connection with the ablation of the summit ice fields [*Mölg et al*., 2009]. The summit of the mountain lies above a trade wind inversion, meaning that the majority of the cloud cover and precipitation occurs on the lower slopes [*Hemp*, 2001]. The precipitation peaks at about 2700–3000 mm at 2200 m elevation on the southern slopes [*Røhr and Killingtveit*, 2003; *Hemp*, 2006c; *Schüler et al*., 2014]. There are two main rainy seasons [*Camberlin and Phillipon*, 2002] known as the "long rains" in April/May and "short rains" in November/December. However, cloud patterns are slightly different between the two. In the short rains, mornings are often clear, but showers and thunderstorms develop in the unstable atmosphere by the afternoon [*Mölg et al*., 2009]. During the long rains there is more widespread persistent precipitation and cloud cover. Outside this period, above 4000 m, skies are typically clear, particularly in the June-July-August-September (JJAS) dry season, which means an extreme radiation climate with intense sunlight by day and clear cold conditions at night. This in turn sets up a thermal circulation on the mountain slopes [*Duane et al*., 2008], which sometimes brings cloud and moisture up the mountain during the afternoon [*Pepin et al*., 2010] only to subside by dusk. Because the mountain is equatorial, sunrise and sunset are at approximately 06:30 and 18:30 East African standard time (EAST) throughout the year.

3.2. Data

In September 2004 a transect of 10 air temperature/relative humidity stations was installed on the southwest (SW) slope (Machame route) ranging from 1800 m to 5800 m in elevation [*Duane et al*., 2008]. This was supplemented by lower stations down to 900 m and another transect of 10 stations on the NE slope (Rongai route) at equivalent elevations to the SW slope in 2012 (see Figure 2). Station details are listed in Table 1. Elevations range from 990 m (Moshi) to 5803 m (summit ice field: Mach10). Hobo Pro DataLoggers

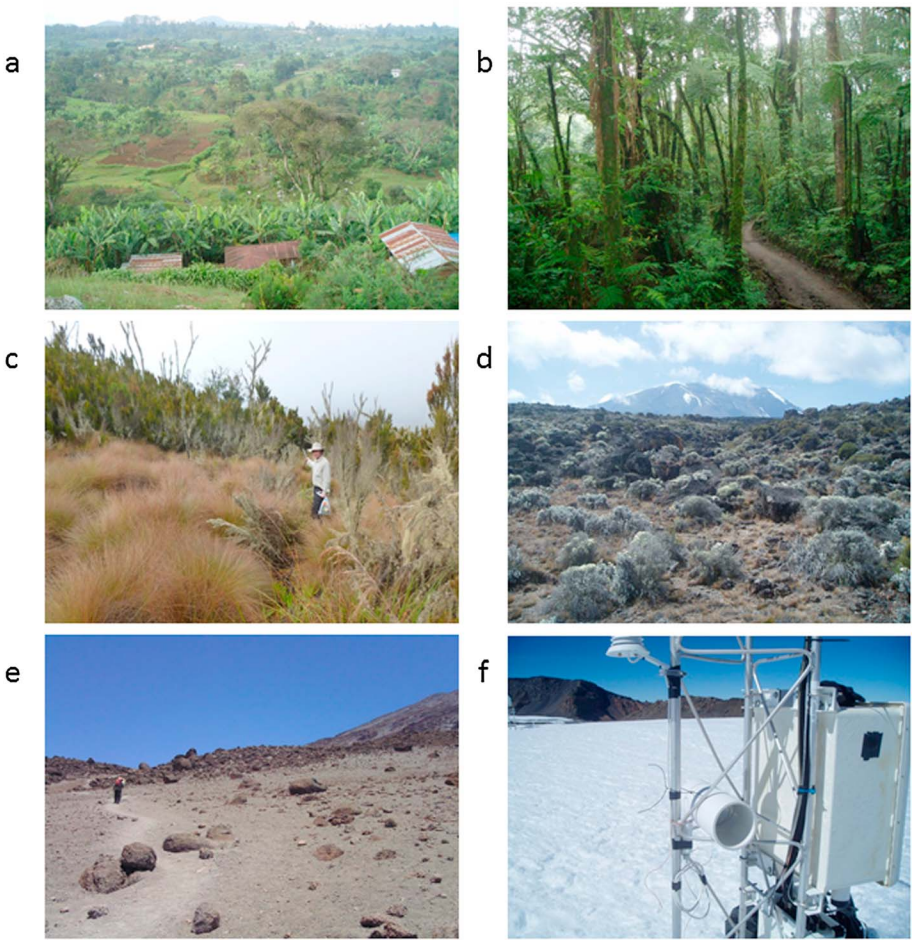

Figure 1. Photographs of the vegetation zones of Kilimanjaro. (a) Cultivated belt (up to 1800 m), (b) montane cloud forest (1800–3100 m), (c) giant heather zone (3100–3900 m), (d) alpine moorland (3900–4500 m), (e) alpine desert (>4500 m), and (f) ice field (summit crater). The data logger screening and setup are illustrated in Figure 1f (horizontal PVc tube fixed to mast).

(U23-001) are installed at 1.5 m above ground level, attached to vegetation on the lower slopes or on tripods above treeline (>4000 m). Sensors are screened with white tubing and orientated (almost) horizontally with the long end facing north-south to ensure that no direct sunlight would enter the tube. A slight angle (<5°) was preferred to avoid air pooling within the tube and increase ventilation. One of the two summit sensors is sited on the northern ice field as part of the weather station operated by the University of Massachusetts used for mass balance research. The other is sited at an equivalent elevation ~200 m away on the ice-free summit of Albion (see Figure 2). At Albion a downward facing sensor installed from 2010-2015 allowed an identification of presence/absence of snow cover, based on reflected shortwave radiation.

Data were recorded every hour (all T_{air} times are EAST:UT +03:00) and records run from September 2004 to September 2015 (11 years) on the SW slope and September 2012 to September 2015 (3 years) on the NE slope. There are some data gaps due to a combination of phased logger installation, vandalism, and logger malfunction (see Table 1), but overall most sites have considerable data of good quality. Data have been evaluated in previous publications [*Duane et al.*, 2008; *Pepin et al.*, 2010] through comparison with National Centers for Environmental Prediction/National Center for Atmospheric Research reanalysis temperatures at equivalent elevations and at the highest site calibrated against the automatic weather station run by the University of Massachusetts. The suitability of this type of data logger for climate monitoring has been assessed by *Whiteman et al.* [2000].

LST is obtained from the MODIS MOD11A2 and MYD11A2 products (Terra and Aqua platforms), which corresponds with 10:30/22:30 local solar time (daytime/nighttime; Terra) and 13:30/01:30 (daytime/nighttime) local

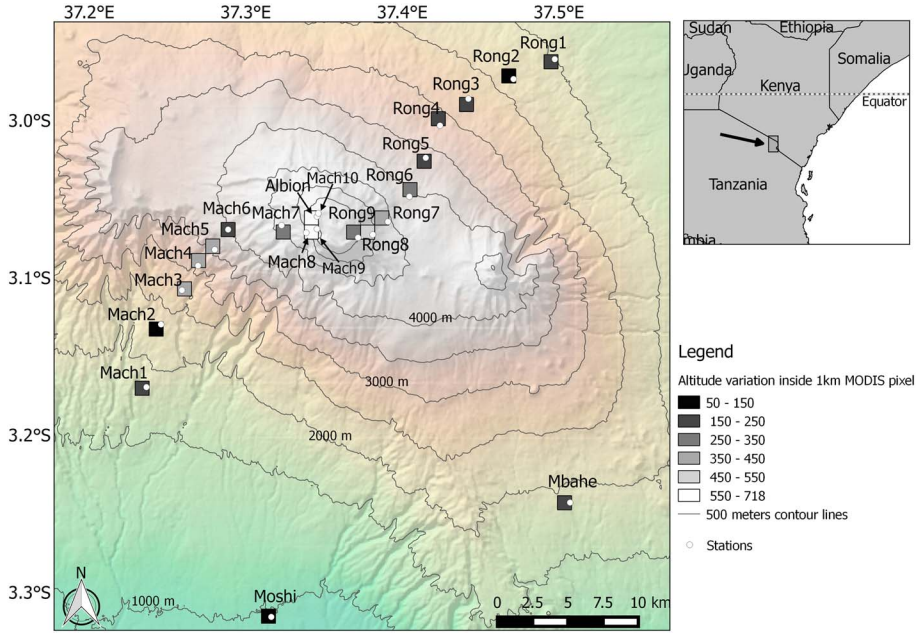

Figure 2. Map showing the location of 22 temperature stations across Kilimanjaro. The SW slope stations are named Mach1–Mach10 (ice field) and the NE stations Rong1–Rong9 (crater wall). Additional stations are situated at Moshi (991 m), Mbahe Farm (1839 m), and Albion (5794 m). The squares represent the 1 km × 1 km MODIS pixels, which are shaded to represent the elevation variation within each pixel. The dots show the position of each station.

solar time (Aqua) (e.g., https://lpdaac.usgs.gov/dataset_discovery/modis/modis_products_table/mod11a2). The data are stored on a 1 km sinusoidal grid. We extracted LST for the relevant pixel for each station (Figure 2). All coordinates were based on universal time meridian and the World Geodetic System 84 ellipsoid. The LST data are produced as an 8 day composite. The composite itself is only derived from clear days within the 8 day period, so in some cloudy periods the composite will be based on only a few days. Occasionally, no value is available because all days were cloudy within the 8 day period. Although a 1 day product exists

Table 1. Station Details

Station	Latitude (°N)	Longitude (°E)	Elevation (m)	Missing Data (%)	Pixel Elevation (m)	Elevation Correction (°C)	Vegetation Zone
Moshi	−3.316	37.316	991	0	989	−0.01	Savannah
Mbahe	−3.243	37.507	1839	0	1903	0.42	Submontane
Mach1	−3.170	37.237	1890	68	1871	−0.12	Rainforest
Mach2	−3.130	37.246	2340	11	2288	−0.34	Rainforest
Mach3	−3.108	37.259	2745	47	2777	0.21	Rainforest
Mach4	−3.092	37.270	3178	24	3137	−0.27	Heather
Mach5	−3.082	37.280	3610	32	3527	−0.54	Heather
Mach6	−3.070	37.289	4039	17	3966	−0.47	Moorland
Mach7	−3.067	37.323	4555	17	4434	−0.79	Moorland
Mach8	−3.071	37.339	4973	26	5134	1.05	Desert
Mach9	−3.069	37.346	5469	7	5134	−2.18	Desert
Mach10	−3.059	37.346	5803	0	5479	−2.11	Ice Field
Albion	−3.061	37.346	5794	0	5479	−2.05	Desert
Rong9	−3.075	37.372	5457	0	5636	1.16	Desert
Rong8	−3.073	37.381	4966	55	5188	1.44	Desert
Rong7	−3.065	37.391	4576	0	4688	0.73	Desert
Rong6	−3.049	37.405	4093	0	3993	−0.65	Moorland
Rong5	−3.023	37.415	3646	33	3662	0.10	Moorland
Rong4	−3.003	37.424	3176	22	3091	−0.55	Heather
Rong3	−2.986	37.442	2764	0	2796	0.21	Heather
Rong2	−2.974	37.471	2338	43	2372	0.22	Rainforest
Rong1	−2.961	37.498	2010	25	2032	0.14	Submontane

(MOD11A1), the high frequency of cloud cover on the slopes of the mountain means that many (sometimes well over 50%) of individual days are missing. The use of the 8 day product avoided this problem. The 8 day product also easily overlapped with the 16 day NDVI product (see below).

Quality control was undertaken using the quality assurance layers provided by the MOD11A2/MYD11A2 products. For each individual pixel the QC layer contains information on measurement quality, emissivity error, and average LST error. We excluded pixels in which LST was not produced due to atmospheric interference or not processed due to poor quality. The clear-sky coverage layer provides an assessment of clear-sky conditions within the 8 day period. Over land MODIS LST is only calculated for pixels at clear-sky conditions at 95% confidence for regions below 2000 m above sea level (asl) and at 66% confidence for regions above 2000 m asl [*Wan*, 2008].

NDVI imagery was obtained from the MOD13Q1 product. This offers 16 day composites at a spatial resolution of 250 m, in which each pixel represents the best quality measurement within a 16 day period [*Justice et al*., 2002]. A data quality control was undertaken considering the MOD13Q1 pixel reliability layer, in which pixels tagged as cloudy were removed.

3.3. Analytical Methods

To compare LST and T_{air} across the range of elevations and ecological zones, air temperatures for 11:00/14:00/23:00/02:00 EAST were compared to 10:30/13:30/22:30/01:30 LST measurements, respectively. Solar noon occurs at 12:30 EAST, and the satellites pass over on average 90 min before/after this. We aggregated T_{air} into the same 8 day periods as the LST measurements. This is likely to be a better approximation when there are many clear days within the composite than when many days are cloudy.

Because some stations on the crater (Mach8/Mach9 and Mach10/Albion) are very close together they fall within the same MODIS pixel. Yet there can be a substantial elevation difference between them. The variability of elevation within each pixel (Figure 2) can be as much as 550–718 m on the crater wall. To account for the potentially large variation within a 1 km pixel, we corrected LST using a standard lapse rate of −6.5°C/km to the elevation of the station (from the mean pixel elevation). The maximum elevation difference was 335 m (Mach9) which translated to a correction of −2.18°C, but most corrections were less than 1°C (see Table 1). We assess error due to intrapixel elevation variability in the discussion.

We calculated LST-T_{air} (hereafter referred to as ΔT). If ΔT is positive it means that the surface is warmer than the air and vice versa. We examined the variation of ΔT with elevation and slope aspect and factors such as season, cloud cover, NDVI, and snow cover. NDVI was provided at 250 m, and the nearest pixel to the station was used (this is a subset of the larger 1 km LST pixel). The 16 day NDVI composite was used to cover two consecutive 8 day periods.

4. Results

4.1. Raw Data

Figures 3 and 4 show isopleth maps of T_{air} and LST, respectively, against elevation (y axis) and time of year (x axis) for the SW slope for (a) day: 13:30 LST and (b) night: 01:30 LST. The 10:30 and 22:30 LST patterns (3 h earlier) are broadly similar but slightly less extreme (not shown). T_{air} (Figure 3) shows a fairly regular decrease with elevation, especially at night (Figure 3b). There is a rapid decrease in daytime temperature (Figure 3a) where the rainforest begins (~1800 m). Temperatures are then fairly stable up until treeline (~3000 m). A weak lapse rate develops around 2500–3000 m in the austral summer and an inversion forms above treeline (3000–3500 m) in the winter (JJA). During the night this complexity disappears and there is a more or less consistent decrease in temperature with elevation. The nighttime freezing level lies around 4300 m and varies little throughout the year. T_{air} is in general slightly lower at night during the austral winter (JJAS), more especially at lower elevations.

The sharp change at the lower forest limit during the day is also picked up by the satellite LST (Figure 4a), with the cloud forest causing considerable cooling in comparison with the warm agricultural zone immediately below. However, there is also considerable surface heating in the alpine moorland zone (4000–4500 m) during the daytime, particularly in the dry seasons (JF and particularly JJAS). LST reaches over 25°C during July–September. At this elevation there is a lack of cloud in these months, and the dry surface heats up

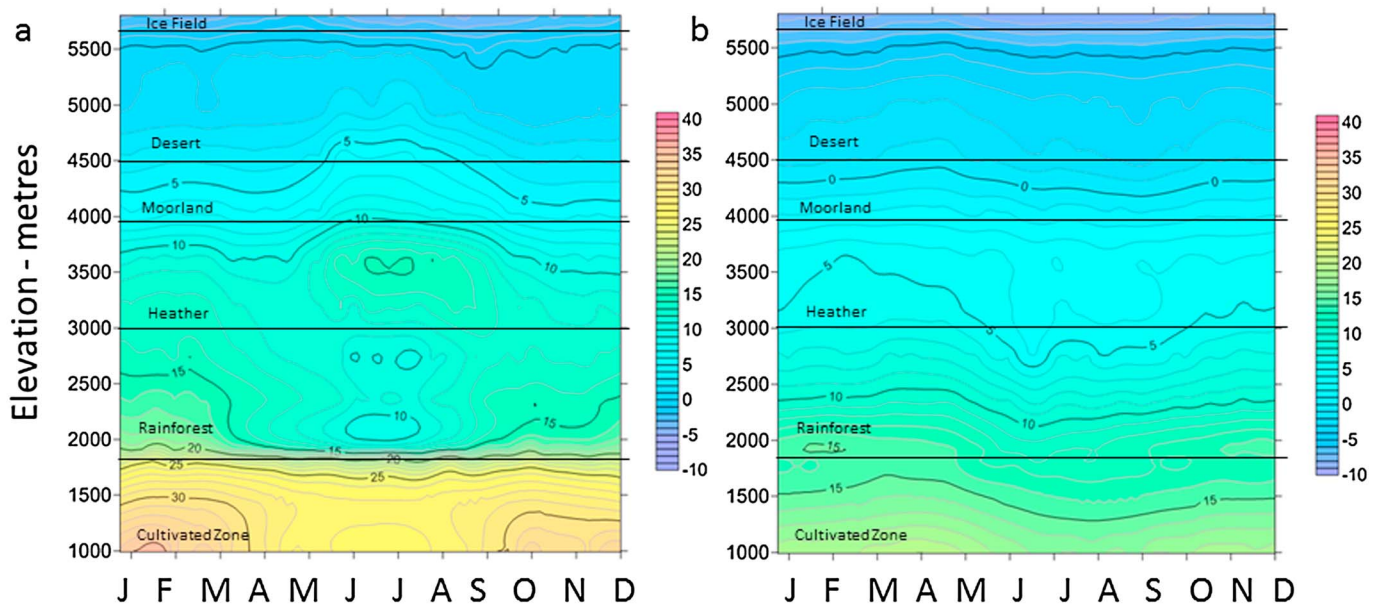

Figure 3. Isopleth diagram showing (a) mean daytime (14:00 EAST) and nighttime (02:00 EAST) T_{air} (SW slope).

effectively due to minimal latent heat flux. The topography also flattens into a plateau (Shira) between 3800 and 4500 m, which would enhance surface heating due to both the mass elevation effect [*De Quervain*, 1904] and overhead Sun angle. A strong inversion therefore develops above treeline during the afternoon. This seasonal contrast in LST remains at the highest elevations (>5000 m), with temperatures during the wet seasons (November-December and March-April-May) being reduced in comparison with the dry seasons. At night LST depends more on elevation alone and is much more regular. Seasonal variations are subdued.

Figure 5 shows a similar plot of ΔT. The most striking feature is the strong variability of daytime ΔT, which reaches over 20°C during the dry seasons at around 4000 m and above. Daytime differences below 3000 m are much smaller, although still predominantly positive. At night, differences tend to be weakly negative,

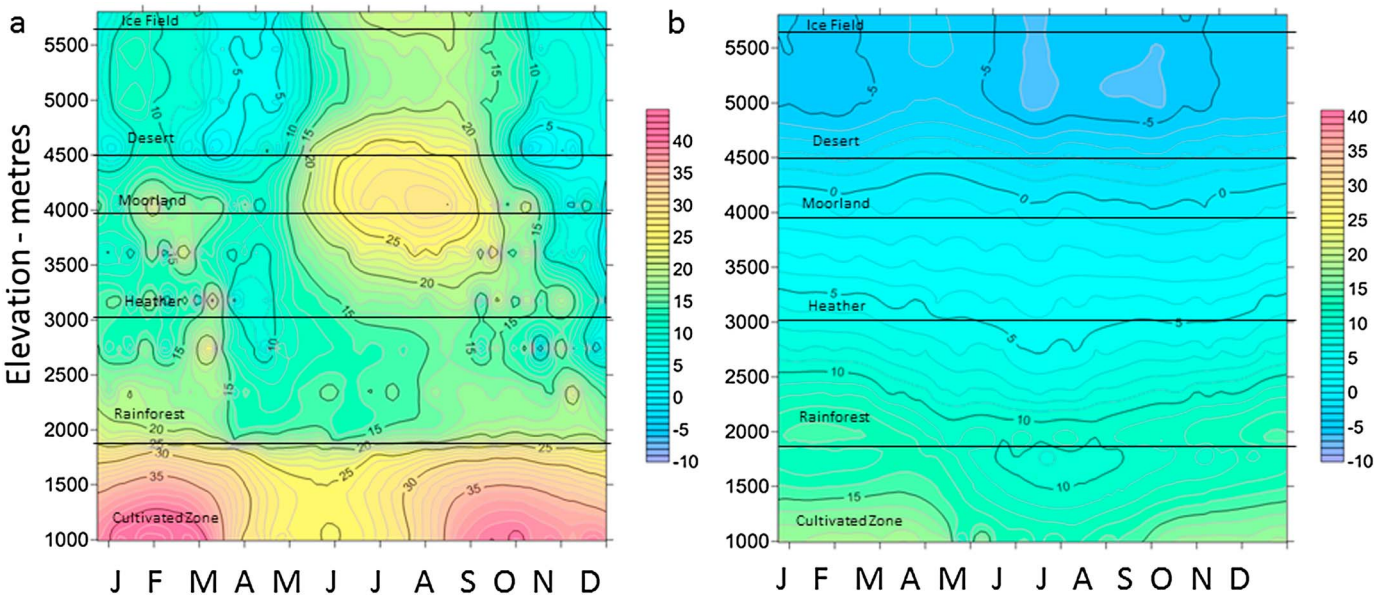

Figure 4. Isopleth diagram showing (a) mean daytime (13:30 LST) and nighttime (01:30 LST) LST from MODIS MYD11A2 (SW slope).

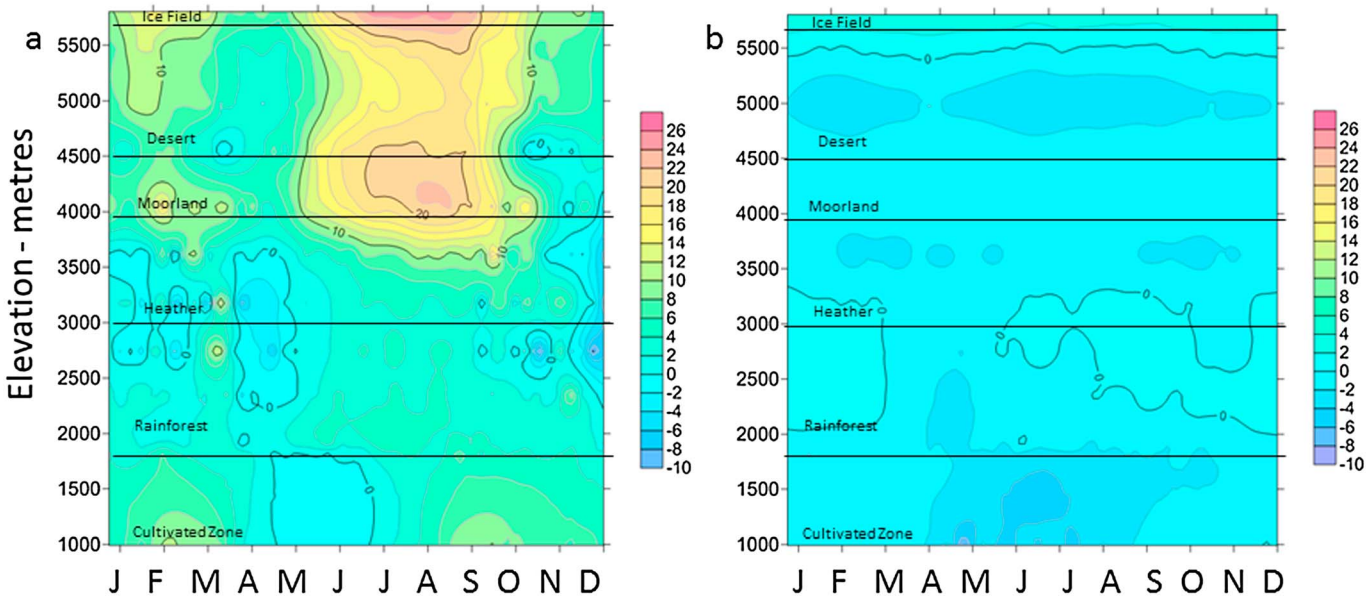

Figure 5. Isopleth diagram showing ΔT (LST minus T_{air}) for (a) 14:00 EAST (13:30 LST) and (b) 02:00 EAST (01:30 LST).

particularly around 5000 m, where there is an absence of cloud. The summit crater and parts of the rainforest however show weak positive differences.

4.2. Patterns of LST Versus T_{air}

Figure 6 plots the correlation (r) between individual 8 day LST and T_{air} observations at each time of day as a function of elevation. The right-hand graph is reversed so the two horizontal axes represent a transect across the mountain from SW to NE. The potential number of 8 day periods on the SW slope is around 500, although n is usually around 300 because of cloud contamination and missing air temperature data. The northeast slope shows more noisy results because there are less data. The most striking pattern is the decrease in correlation at high elevations during the day (11:00 and 14:00 EAST) on both slopes. At night the decrease in correlation disappears and there is a less systematic deterioration of r with elevation.

The mean LST-air temperature difference (ΔT) is plotted in Figure 7 in a similar format. Again, there are large contrasts between day and night. During the day LST tends to be warmer than T_{air} (positive ΔT), although differences are fairly small on the lower forested slopes (particularly in the cloud forest around 2000 m). ΔT increases rapidly above treeline (3100 m), peaking on the higher slopes around 5000 m. On the northeast slope mean differences at 14:00 EAST exceed 20°C at Rong8 (4966 m). Even on the southwest slope differences are significant (between 5 and 15°C). At night the contrast between the slopes disappears, and the LST is uniformly colder than the air but not by a large amount. The elevational gradient in the difference also disappears at night. These distinctive patterns show that LST and T_{air} are certainly not the same measurement.

Figure 8 breaks down the LST versus T_{air} correlation for clear (4–7 clear days; Figures 8a and 8b) and cloudy (0–3 clear days; Figures 8c and 8d) composites separately. The deterioration of correlation with elevation is stark during clear daytime composites on both slopes (Figures 8a and 8b), but there is a less consistent drop at night and perhaps on the NE slope in general. Differences between clear and cloudy periods are subtle.

4.3. Seasonal Patterns in ΔT

Figures 9 and 10 show the seasonal patterns of ΔT at a selection of low/high-elevation sites, respectively. During the day (11:00 and 14:00 EAST), differences are much larger during the dry seasons when solar heating is strong and the surfaces drier. At Moshi (on the plains) the peaks in February/March and September/October correspond with both the Sun being directly overhead at noon and dry seasons. In the rainforest zone (Mach2 and Rong2) seasonal changes are more subdued. Seasonal changes are also smaller at night in general at all sites. Perhaps against intuition, the biggest differences (most negative ΔT) are often

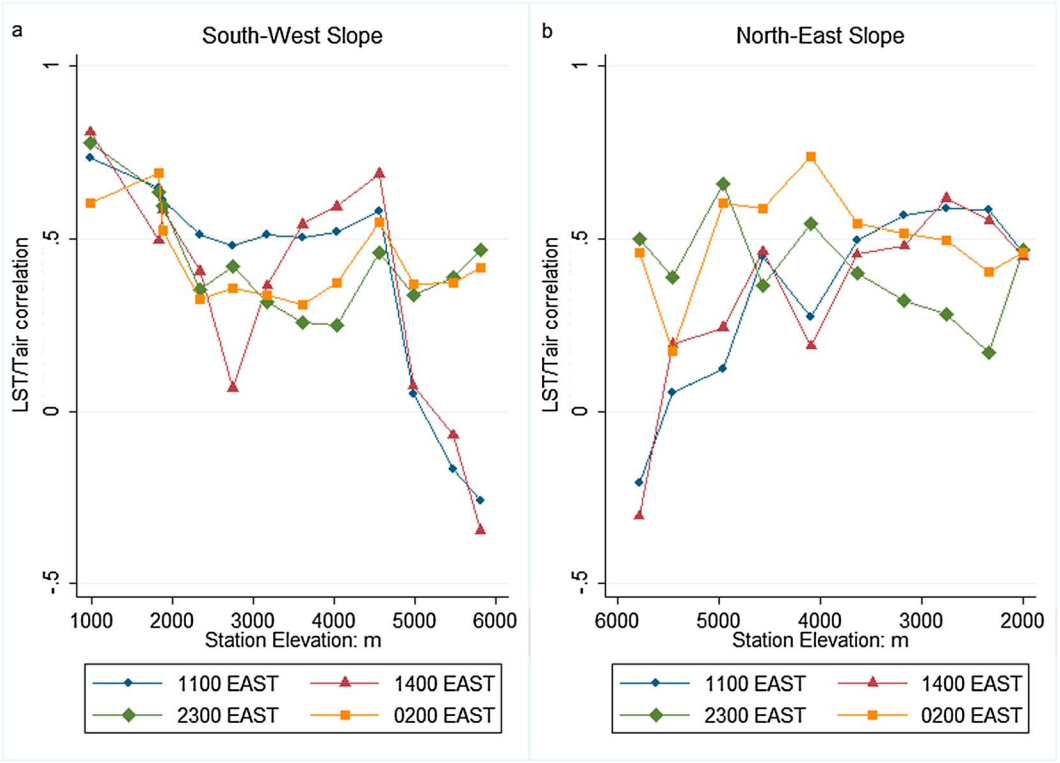

Figure 6. (a and b) Correlation between LST and T_{air} at each station versus elevation.

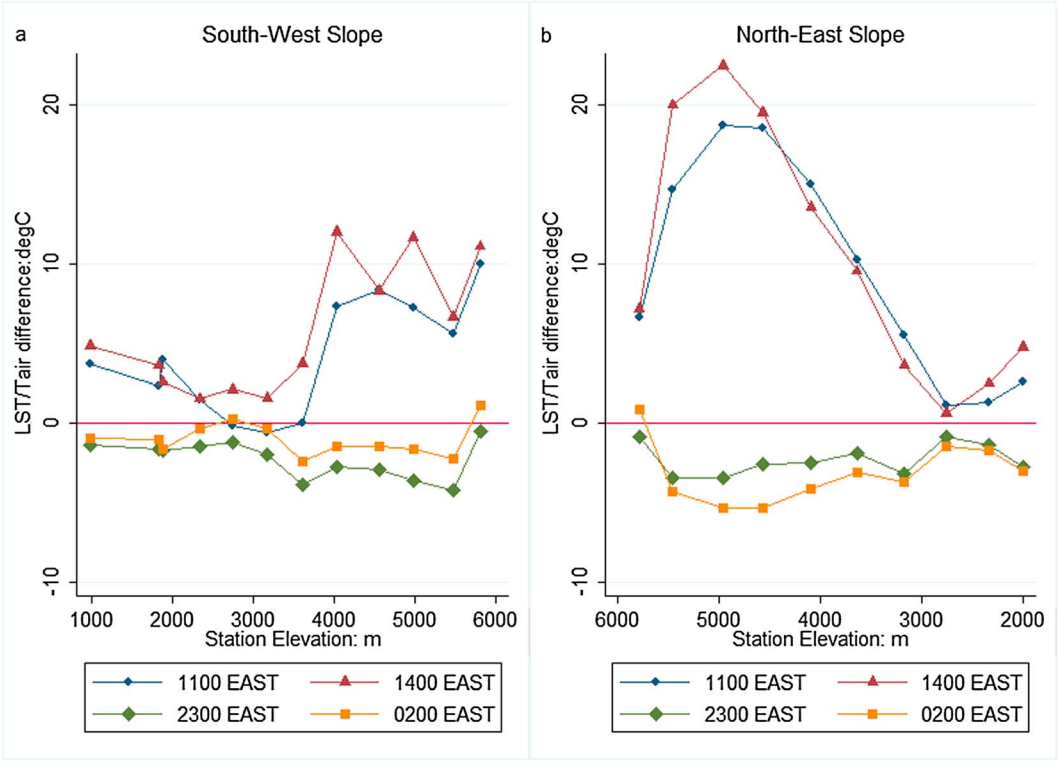

Figure 7. (a and b) Mean LST/air temperature difference (ΔT) versus elevation for 4 times of day. The 95% confidence intervals (error bars not shown) average ±0.67°C (11:00), ±0.86°C (14:00), ±0.20°C (23:00), and ±0.18°C (02:00 EAST) across all stations.

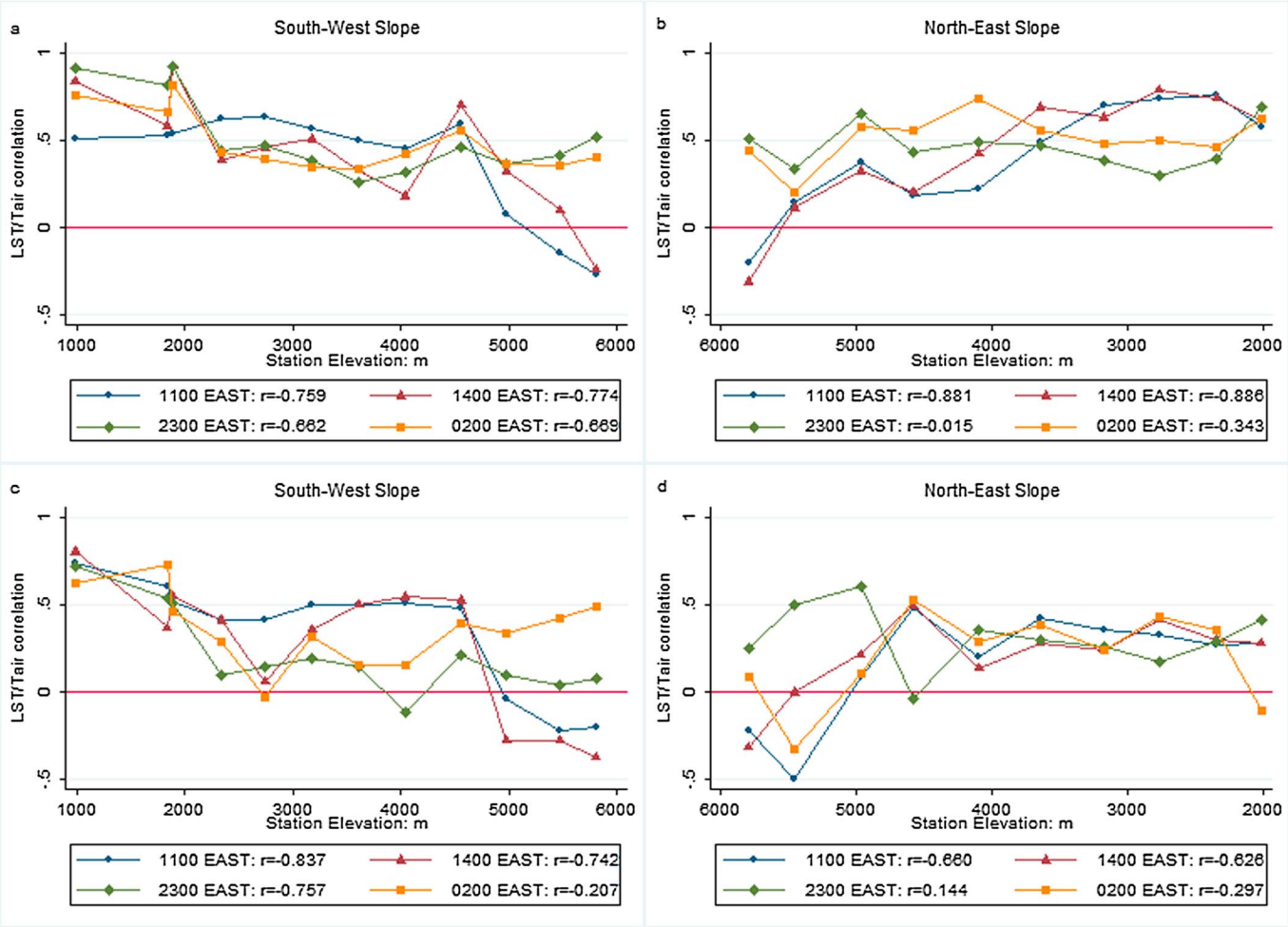

Figure 8. Effect of cloud on the deterioration of the LST/T_{air} correlation with elevation. (a) Clear composite (4–7 clear days) SW slope, (b) clear composite (4–7 clear days) NE slope, (c) cloudy composite (1–3 clear nights) SW slope, and (d) cloudy composite (1–3 clear nights) NE slope.

during the wet seasons (May or November) at the low-elevation sites, the reason for which is unclear because surface radiation loss should be limited by moist surfaces. At higher elevations (Figure 10) the influence of wet and dry seasons becomes more important. At Mach7, Mach10, and Albion, the short rains (November/December) mark a time when convective cloud build up and precipitation is much more likely at crater level. This appears to reduce daytime ΔT. There is a large contrast between the two dry periods, with the least cloudy JJAS period mostly responsible for the large daytime ΔT values in excess of 20°C. Similar to low-elevation sites, nighttime ΔT shows much less seasonal variation in general.

In summary the differences between LST and T_{air} show strong patterns controlled by the frequency of cloud cover and its interaction with the changing radiation balance over the course of the day and year. In future sections we examine how seasonal and short-term (intraweekly) changes in moisture and relative humidity, vegetation, and snow cover can help explain the variation in ΔT.

4.4. Effect of Cloud Cover and Relative Humidity

Figure 11 plots ΔT against the number of cloud-free days within the composite for two SW slope sites during the day (11:00 EAST; Figures 11a and 11b) and night (23:00 EAST; Figures 11c and 11d). The 14:00/02:00 EAST patterns are broadly similar (not shown). The *x* axis represents the number of clear days within the composite (more cloudy conditions on the left). Mach2 is in the rainforest, and Mach8 in the alpine desert. Accepting a null hypothesis that cloud has no effect on ΔT, then ΔT should become less variable and closer to zero as the number of clear days increases, purely because LST is based on more of the same days as T_{air} (which is based

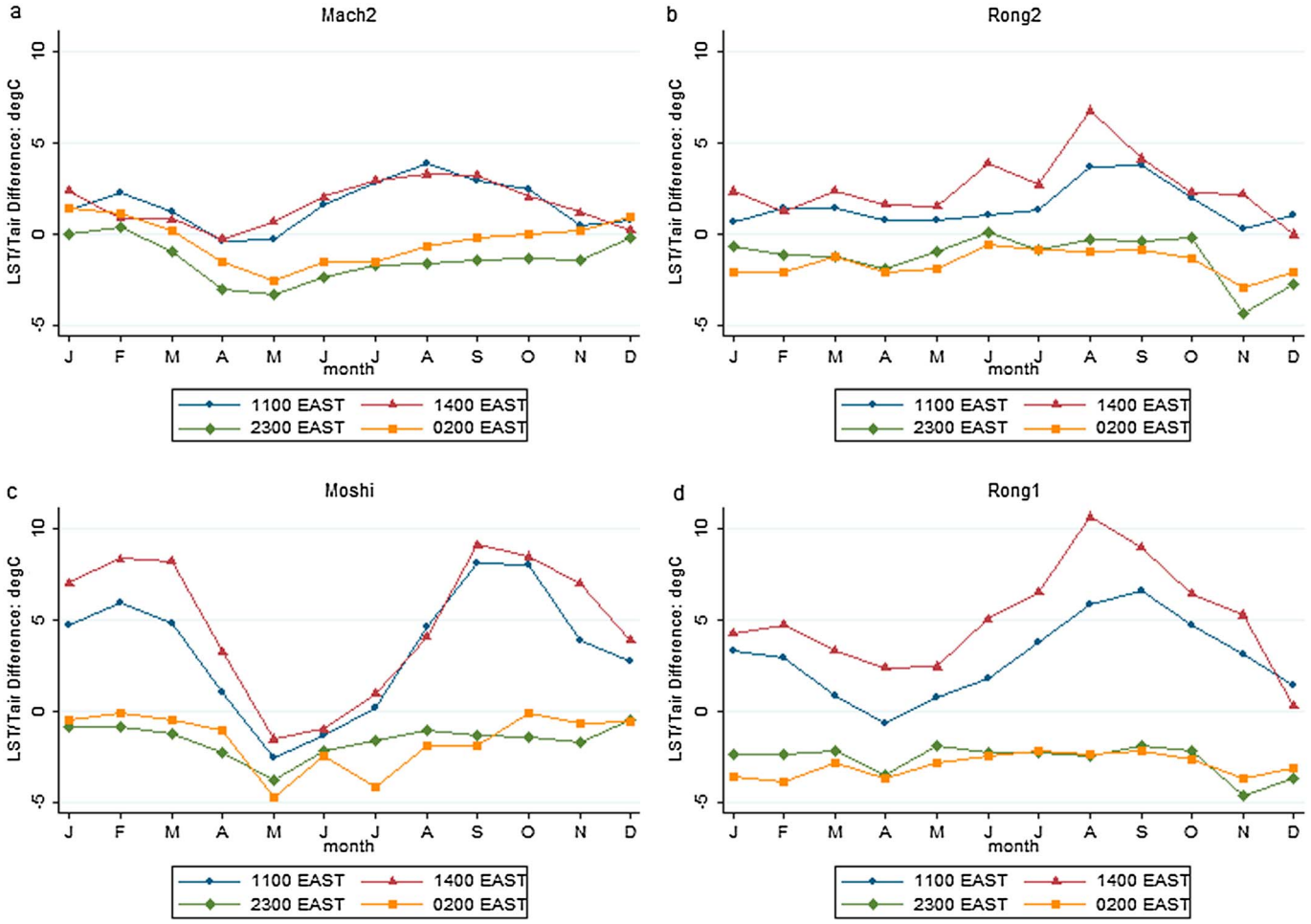

Figure 9. Seasonal and diurnal patterns in mean ΔT at (a) Mach2 (rainforest: SW slope), (b) Rong2 (rainforest: NE slope), (c) Moshi (plains SW of mountain), and (d) Rong1 (plains NE of mountain). Mean 95% confidence intervals (error bars not shown) are ±0.895°C (Mach2), ±1.353°C (Rong2), ±1.277°C (Moshi), and ±1.171°C (Rong1).

on all 8 days). However, although the variance in ΔT decreases (probably due to increasingly data similarity) the size of the daytime difference tends to increase. Thus, under composites with more frequent clear-sky conditions (stronger radiation input) the surface tends to heat up more in comparison with the air, particularly at the higher site (Mach8). At night the variance in ΔT also decreases for clearer composites. However, the mean difference does not always become more negative (which we would expect based on rapid surface cooling under clear skies). At some sites such as Mach2 in the rainforest the difference becomes smaller (closer to zero), but at others (Mach8) it becomes larger (more negative). Thus, differences between sites impact on nighttime cloud effects on ΔT.

The data loggers also recorded relative humidity as well as temperature. Apart from one or two exceptions, there are strong negative correlations between daytime ΔT and relative humidity (%) at many locations (Table 2). The left-hand columns represent the correlation based on raw 8 day values and the right-hand columns the correlation remaining when the common seasonal cycles in both ΔT and relative humidity have been removed. Although correlations tend to be stronger using the raw values rather than anomalies, the difference is small near the summit of the mountain, meaning that the seasonal cycle is not responsible for the negative correlations between ΔT and relative humidity (RH) above 4500 m. Strong interweekly variability in moisture caused by synoptic variations must therefore account for much of the change in ΔT on the summit crater and at some sites on the NE slope (e.g., Rong4, Rong5, and Rong7). More humid conditions (which will mean a much higher likelihood of cloud cover at the elevation of the station) lead to subdued differences. At Mach7 and Rong7 (4555 m) for example nearly 50% of the variance in the

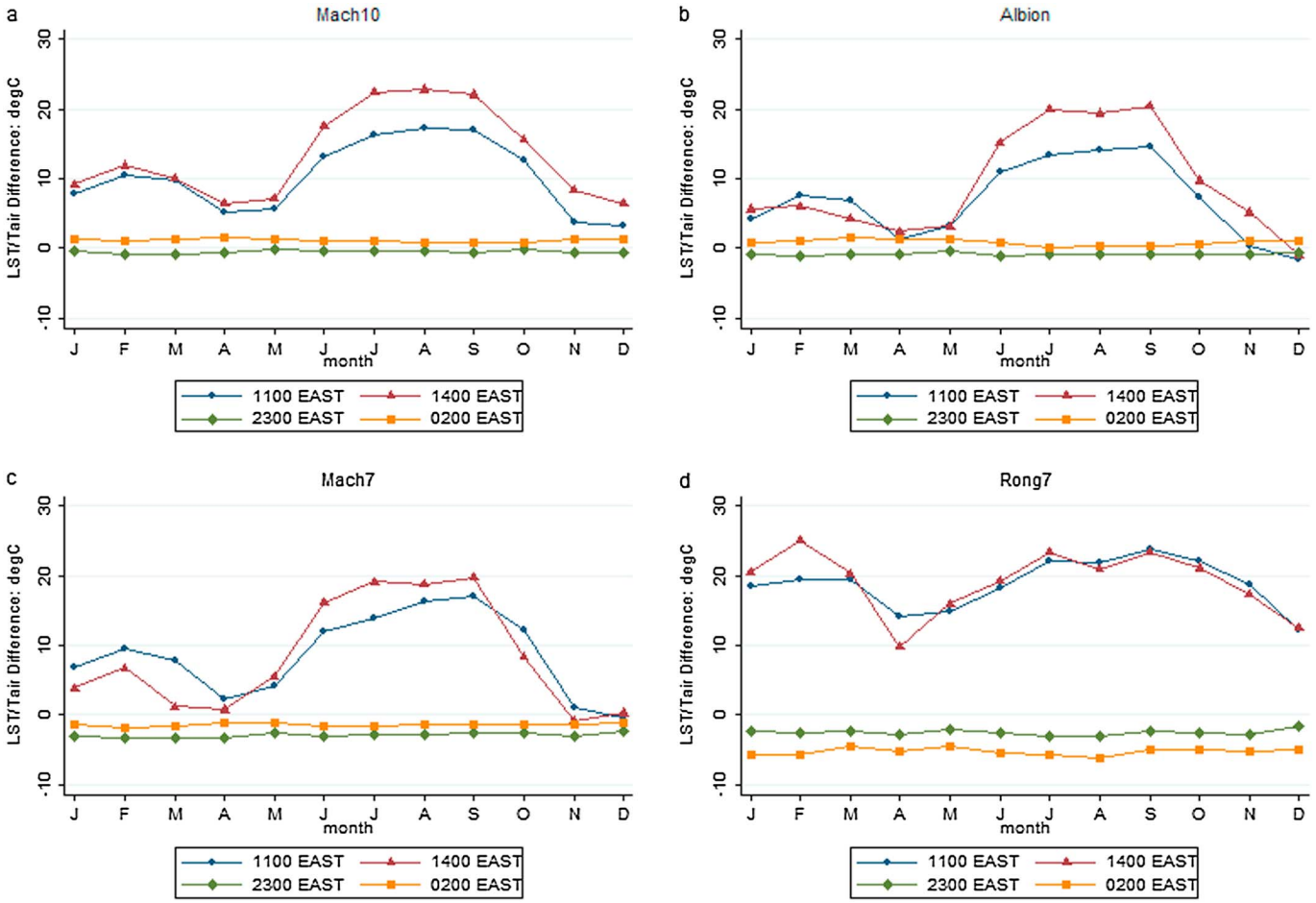

Figure 10. Similar to Figure 9 but for high-elevation stations: (a) Mach10 (crater ice field), (b) Albion (crater desert), (c) Mach7 (alpine moorland: SW slope), and (d) Rong7 (alpine desert: NE slope). Mean 95% confidence intervals (error bars not shown) are ±0.973°C (Mach10), ±1.347°C (Albion), ±1.155°C (Mach7), and ±2.072°C (Rong7).

difference can be accounted for by afternoon RH, and a significant relationship remains ($p < 0.01$) when annual cycles have been removed.

4.5. Effect of Surface Characteristics (Vegetation and Snow Cover)

The relationship between NDVI MOD13Q1 and daytime ΔT is shown in Figure 12 for two bottom and two high-level sites on each transect. In the lowlands (Moshi and Rong1) there are strong negative relationships, with increased NDVI (greener vegetation) reducing ΔT as in previous studies. At some high-level sites (but not Mach10 on the ice field) the relationship reverses. However, NDVI is very low at the highest elevations (there is no vegetation) and is more likely to be influenced by snow cover. Table 2 (right-hand column) lists the correlation between daytime ΔT and NDVI MOD13Q1 for all locations. Correlations tend to be more significant on the SW slope, but this is probably because there is a larger sample size. At night there was an absence of significant correlations with MOD13Q1 (not shown).

At Albion where snow cover is sporadic, we assessed the effect of snow cover on the relationships between NDVI and ΔT and on the correlation between LST and T_{air}. Snow cover was estimated to be present if reflected shortwave radiation at 11:00 EAST exceeded 237 W/m^2 (around 43% of days). Although there was no significant difference in the LST/T_{air} correlation between snowy (4 or more days) and non-snowy (less than 4 days) composites at Albion, LST was reduced much more than T_{air} by the presence of snow cover (Figure 13a). There is also a significant difference (two-tailed t test: $p = 0.0012$) between NDVI values recorded under conditions of snow cover versus snow-free composites (Figure 13b), with more negative values

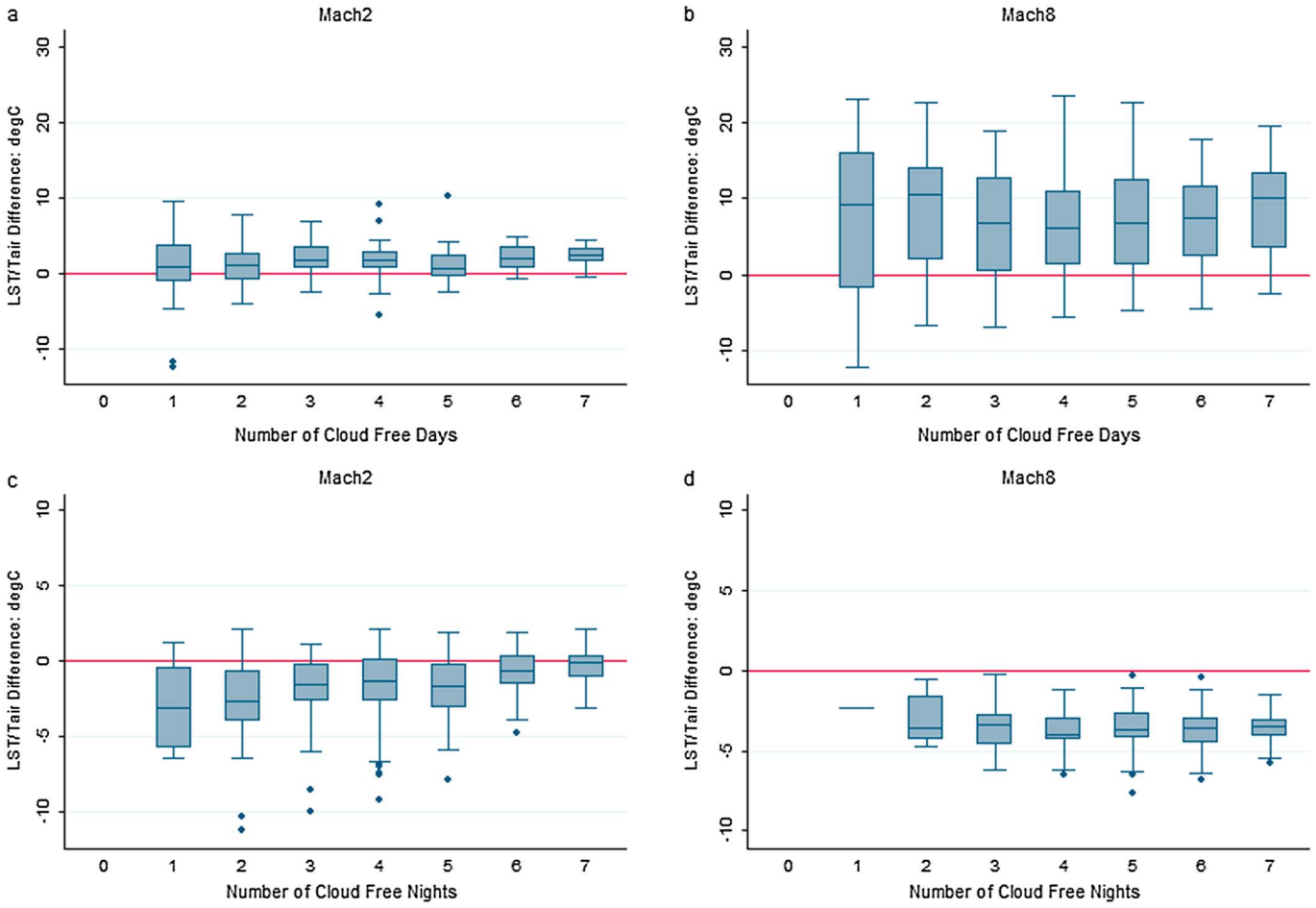

Figure 11. Cloud effects on ΔT for two sites: (a) Mach2 (2340 m) 11:00 EAST and (b) Mach8 (4973 m) 11:00 EAST and (c) Mach2 23:00 EAST and (d) Mach8 23:00 EAST. The number of cloud-free days/nights within the 8 day composite is represented on the *x* axis.

representative of snowy conditions. When mean NDVI at a station falls below 0.1 the daytime correlation between LST and T_{air} also falls dramatically (figure not shown).

5. Discussion

The rapid deterioration (and even reversal) in correlation between LST and T_{air} at high elevations is important to the debate on elevation-dependent warming. Although satellite data have great potential to complement air temperature data at high elevations [*Qin et al*., 2009], unfortunately, LST is increasingly poorly related to T_{air} as elevation increases. One likely cause is that the surface radiation balance becomes increasingly variable both temporally (as solar geometry changes) and spatially (as factors such as aspect, topographic screening, and land surface contrasts become increasingly important in high mountains) [*Barry*, 2008]. The low air density at high elevations means that despite rapid surface response to energy balance fluctuation, this is not transferred readily into T_{air} at screen level, which is more decoupled from the surface response (LST) than it would be at sea level. At extremely high elevations a negative relationship between LST and T_{air} could arise because increased moisture warms the air through increased longwave emission [*Rangwala et al*., 2009], but cools the surface through increased likelihood of snow cover, and increased latent heat flux.

Intense sunlight at high elevations can warm the surface far above T_{air}, which explains the daytime increase in ΔT with elevation. Although the rate at which direct radiation input increases with elevation depends on solar angle and atmospheric transmissivity [*Kastrov*, 1956; cited by *Barry*, 2008], solar radiation intensity at the summit of Kilimanjaro (~6000 m) is typically 5–12% greater than at sea level [*Barry*, 2008] and frequently exceeds 1000 W/m^2 [*Mölg et al*., 2008] on the northern ice field. The NE aspect of the mountain faces the Sun in the

Table 2. Daytime Correlations Between Relative Humidity, NDVI (as Measured by MOD13Q1) and LST-T_{air}

	Relative Humidity (11:00 EAST)			Relative Humidity (14:00 EAST)			MOD13Q1 (11:00 EAST)	
Station	*n*	Correlation	Correlation[a]	*n*	Correlation	Correlation[a]	*n*	Correlation
Moshi	168	−0.471***	−0.080	184	−0.610***	−0.226***	91	−0.613***
Mbahe	181	0.009	0.104	182	−0.142*	−0.006	94	−0.160
Mach1	110	−0.159***	−0.206**	108	0.265***	0.252***	91	0.251**
Mach2	331	−0.307***	−0.244***	202	0.063	0.076	103	0.235***
Mach3	230	0.017***	0.043	110	0.218**	0.184*	135	0.235***
Mach4	356	−0.287***	−0.185***	174	−0.208***	−0.030	194	0.019
Mach5	345	−0.402***	−0.167***	197	−0.367***	−0.018	176	0.135*
Mach6	337	−0.570***	−0.309***	227	−0.629***	−0.234**	243	0.266***
Mach7	322	−0.602***	−0.326***	268	−0.689***	−0.221***	244	0.291***
Mach8	301	−0.530***	−0.288***	292	−0.352***	−0.052	205	0.537***
Mach9	429	−0.202***	−0.076	414	−0.126**	0.037	213	0.361***
Mach10	501	−0.353***	−0.388***	490	−0.311***	−0.336***	199	−0.234***
Albion	225	−0.317***	−0.302***	220	−0.300***	−0.229***	84	0.093
Rong9	110	−0.277***	−0.239***	110	−0.404***	−0.322***	31	0.225
Rong8	94	0.084	0.185	90	−0.294***	−0.187*	14	−0.226
Rong7	136	−0.625***	−0.602***	130	−0.526***	−0.479***	48	0.064
Rong6	70	−0.551***	−0.427***	66	−0.340***	−0.168	41	−0.246
Rong5	117	−0.511***	−0.359***	101	−0.497***	−0.357***	31	−0.209
Rong4	131	−0.612***	−0.513***	113	−0.433***	−0.392***	36	−0.033
Rong3	136	−0.212**	−0.104	110	−0.093	−0.033	50	0.025
Rong2	102	−0.051	0.029	95	−0.189*	−0.219**	28	−0.102
Rong1	121	−0.313***	−0.230***	112	−0.251***	−0.321***	35	−0.575***

[a]Correlation with seasonal cycles removed. The left hand correlations are between raw values.
*Significant at $p<0.10$. **Significant at $p<0.05$. ***Significant at $p<0.01$.

morning, explaining why differences between LST and T_{air} are slightly smaller on the SW aspect at both 11:00 and 14:00 EAST. Although the SW slope should heat up in the afternoon, convective cloud limits afternoon heating [*Pepin et al.*, 2010; *Mölg et al.*, 2009]. Although daytime values of ΔT can exceed 20°C, similar results have been obtained in other studies under less extreme radiative conditions [*Shamir and Georgakakos*, 2014], and we have no reason to suspect that these values are erroneous.

Because surface heating is dependent on direct radiation input, any patchy cloud cover, or any topographic screening will change LST but have less influence on T_{air}. We examined the influence of changing pixel at the highest-elevation sites (Mach10 and Albion) to the neighboring 1 km square (which could be topographically contrasting), and in some cases differences in LST were substantial (>10°C). It is informative to compare this with error due to altitude variation within a pixel (up to ±350 m). In the worst case (the western crater wall) this translates to an error of ±2.28°C, assuming a standard lapse rate of −6.5°C/km [*Maeda*, 2014]. However, elevation error is still insignificant compared with mean values of ΔT, which can reach over 20°C (Figure 10) on the higher slopes, and compared with interpixel variability of LST due to differential aspect/radiative load (>10°C). Thus, small differences in positioning of satellite measurements over time (i.e., because of changing cloud cover) would create significant changes in LST. Thus, there is a lot of small-scale noise in the LST record, which would need to be corrected for if satellite data were to be used to represent high-elevation temperature trends over large areas.

The strong negative relationship between daytime ΔT and relative humidity means that moister air leads to reduced surface heating. This pattern is particularly strong at midlevel stations on the SW slope (i.e., Mach6, Mach7, and Mach8), where there is large day to day variance in the amount of cloud cover and moisture brought up the slope through the thermal circulation mechanism [*Duane et al.*, 2008]. The strong relationship of ΔT with atmospheric moisture opens up the possibility, at least in theory, of using humidity measurements to predict ΔT and subsequently adjust satellite temperatures to predict air temperatures, if atmospheric soundings were available. However, previous work on Kilimanjaro [*Pepin et al.*, 2010] has demonstrated large differences between in situ moisture (at screen level from surface stations) and free air measurements at the same elevation (from reanalyses and radiosonde ascents), and such differences would complicate the process.

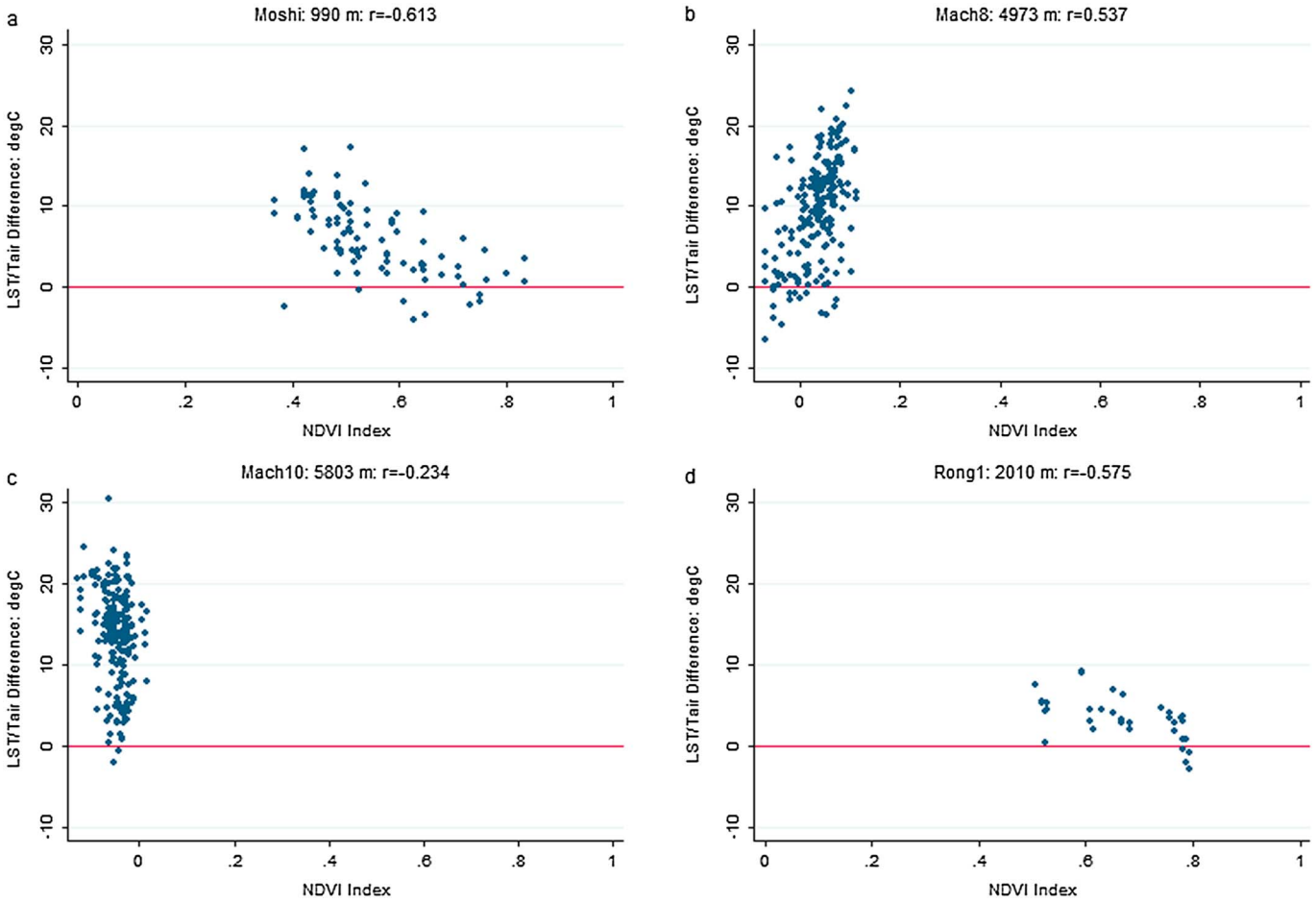

Figure 12. Correlations between mean daytime ΔT and NDVI (as measured by MOD13Q1) for four sites: (a) Moshi (990 m), (b) Mach8 (4973 m), (c) Mach10 (5803 m), and (d) Rong1 (2010 m).

Healthy vegetation can also dampen daytime surface warming, through increasing the latent heat flux. ΔT was smaller and more consistent at the lower vegetated sites than higher up the mountain. However, even at lower sites the surface still warmed during the day in comparison with T_{air}. In the cloud forest the satellite is measuring the canopy surface temperature (above the temperature sensor) as the effective radiative surface. NDVI showed a strong negative correlation with ΔT at the low-level sites, with greener vegetation (higher index) leading to relative surface cooling as supported by previous studies [*Nemani and Running*, 1989; *Wenbin et al*., 2013]. However, at the highest elevations, where vegetation is reduced or absent, the biophysical interpretation of NDVI variation is difficult, and the relationship reverses. The main source of variability in surface properties at the higher stations (excluding the ice field itself) is transient snow cover. At Albion snow cover occurred around 43% of the time, and although it did not appear to have a strong influence on the LST/T_{air} correlation, it did reduce LST in preference to T_{air} and thus reduce ΔT. NDVI also reduces under conditions of snow cover, and this probably reverses or weakens the relationship between ΔT and NDVI at some higher stations. Unfortunately, reliable snow cover data needed for a more extensive analysis are not available at a fine enough resolution, both Mach10 (permanent ice) and Albion (transient snow cover) falling in the same pixel for example, but snow effects should be a focus for further research.

At night it would be expected that the surface would cool more at higher elevations (since radiation escapes more effectively into space), but although LST is consistently lower than T_{air}, there is no strong elevational signal in ΔT. More consistent differences means that using satellite data as a proxy for air temperature could therefore be much more reliable, and since many studies have shown nighttime warming rates to be both faster globally than mean temperatures [*Karl et al*., 1993] and also to show more of an elevational-dependent signal [*Rangwala and Miller*, 2012], it would be wise to first use satellite temperatures to examine trends in T_{min} at high elevations.

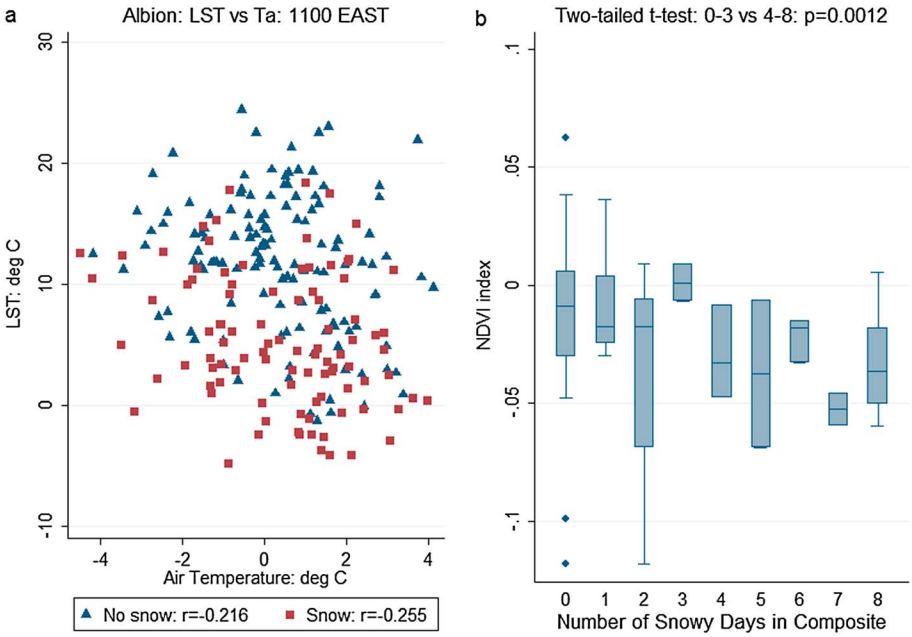

Figure 13. (a) LST versus T_{air} at Albion station (5794 m) separated by snow cover presence/absence and (b) NDVI at Albion versus number of snowy days in 8 day composite.

Despite elevation-dependent warming providing a strong context for our research, we have not analyzed temporal trends in LST, T_{air}, or ΔT in this study because the length of the record (11 years) is not long enough to draw robust conclusions, but our findings show that LST and T_{air} require careful comparison before LST is used as a proxy for T_{air} in mountainous terrain.

6. Conclusions

Our study has shown that there are large instantaneous differences between LST as measured by the MODIS MOD11A2/MYD11A2 products at 1 km resolution and equivalent T_{air} measured from in situ weather stations. These differences are variable, particularly during the daytime, and the predictability of the differences tends to reduce with elevation. Both relative humidity and vegetation state can be used to some extent to predict ΔT, but at extremely high elevations this method is less successful. Our study is only based on one transect on one tropical mountain, but it is likely to represent the challenges of using LST to represent T_{air} in other high-elevation areas worldwide, with similar changes in vegetation, moisture, and snow cover with elevation. Treelines and snowlines are of universal importance on mountains worldwide, so the large-scale controls on ΔT in this study are broadly similar to those in all mountains. High-elevation radiation balance is controlled by the fundamental laws of physics [*Ohmura*, 2012], so the results shown here would be expected to occur in other mountain ranges. There is no permanent snowline on Kilimanjaro (snow is transient, even on the summit crater), and further research is required on the role of persistent deep snow cover on the climatologies of LST and T_{air} [e.g., *Hachem et al*., 2012]. The general conclusion that LST becomes more different from air temperature as elevation increases is an important one, because careful validation is therefore required before such LST records can reliably be used to assess elevational dependency of T_{air} warming rates in mountainous areas.

Acknowledgments
Eduardo Maeda is currently funded by a research grant from the Academy of Finland. We thank the Natural Environment Research Council (NERC) for providing funding (NE/J013366/1) for the field campaign on Kilimanjaro and the expansion of the weather station network to cover the northeastern slope. We thank Doug Hardy, Mark Losleben, Martin Schaefer, Gary Pike, Andrew Day, Simon Mtuy, and staff at Summit Expeditions and Nomadic Experience for their help in the field. We acknowledge the help of staff at TAWIRI (Tanzania Wildlife Research Institute) in granting permission for this research and, along with TANAPA (Tanzania National Parks), providing access to the Kilimanjaro National Park. Kilimanjaro air temperature data for 2012–2015 are archived with NERC at the Centre for Environmental Data Analysis (http://cedadocs.badc.rl.ac.uk/). The MODIS MOD11A2/MYD11A2 data products were retrieved from the online Data Pool, courtesy of the NASA Land Processes Distributed Active Archive Center, USGS/Earth Resources Observation and Science Center, Sioux Falls, SD (https://lpdaac.usgs.gov/data_access/data_pool). There are no conflicts of interest.

References

Barry, R. G. (2008), *Mountain Weather and Climate*, 3rd ed., 506 pp., Cambridge Univ. Press, U. K.
Benali, A., A. C. Carvalho, J. P. Nunes, N. Carvalhais, and A. Santos (2012), Estimating air surface temperature in Portugal using MODIS LST data, *Remote Sens. Environ.*, *124*, 108–121.
Camberlin, P., and N. Phillipon (2002), The East African March–May rainy season: Associated atmospheric dynamics and predictability over the 1968–97 period, *JNl Clim.*, *15*, 1002–1019.
Ceppi, P., S. C. Scherrer, A. M. Fischer, and C. Appenzeller (2010), Revisiting Swiss temperature trends 1959–2008, *Int. J. Climatol.*, *32*, 203–213.
Coll, C., Z. Wan, and J. M. Galve (2009), Temperature-based and radiance-based validations of the v5 MODIS land surface temperature product, *J. Geophys. Res.*, *114*, D20102, doi:10.1029/2009JD012038.
Coutts, H. H. (1969), Rainfall of the Kilimanjaro area, *Weather*, *24*, 66–69.

Daly, C., D. R. Conklin, and M. H. Unsworth (2010), Local atmospheric decoupling in complex topography alters climate change impacts, *Int. J. Climatol.*, *30*, 1857–1864.
De Quervain, A. D. (1904), Die Hebung der atmosphärischen Isothermenin der Schweizer Alpen und ihre Beziehung zu deren Höhengrenzen, *Gerlands Beitrage zur Geophysik*, *6*, 481–533.
Diaz, H. F., and R. S. Bradley (1997), Temperature variations during the last century at high elevation sites, *Clim. Change*, *36*, 253–279.
Duane, W. J., N. C. Pepin, M. L. Losleben, and D. R. Hardy (2008), General characteristics of temperature and humidity variability on Kilimanjaro, Tanzania, *Arct. Antarct. Alp. Res.*, *40*, 323–334.
Fairman, J. G. Jr, U. S. Nair, S. A. Christopher, and T. Mölg (2011), Land use change impacts on regional climate over Kilimanjaro, *J Geophys Res.*, *116*, D03110, doi:10.1029/2010JD014712.
Hachem, S., C. R. Duguay, and M. Allard (2012), Comparison of MODIS-derived land surface temperatures with ground surface and air temperature measurements in continuous permafrost terrain, *Cryosphere*, *6*(1), 51–69.
Hartmann, D. L., et al. (2013), Observations: Atmosphere and surface, in *Climate Change 2013: The Physical Science Basis. Contribution of Working Group I to the Fifth Assessment Report of the Intergovernmental Panel on Climate Change*, edited by T. F. Stocker et al., Cambridge Univ. Press, Cambridge, U. K., and New York.
Hastenrath, S. (1991), *Climate Dynamics of the Tropics*, Kluwer, Dordrecht, Boston, London.
Hastenrath, S., and L. Greischar (1997), Glacier recession on Kilimanjaro, East Africa, 1912-89, *J. Glaciol.*, *43*, 455–459.
Hemp, A. (2001), Ecology of the pteridophytes on the southern slopes of Mt. Kilimanjaro. Part II: Habitat selection, *Plant Biol.*, *3*, 493–523.
Hemp, A. (2005), Climate change-driven forest fires marginalize the impact of ice cap wasting on Kilimanjaro, *Global Change Biol.*, *11*, 1013–1023.
Hemp, A. (2006a), Continuum or zonation? Altitudinal gradients in the forest vegetation of Mt. Kilimanjaro, *Plant Ecol.*, *184*, 27–42.
Hemp, A. (2006b), The banana forests of Kilimanjaro: Biodiversity and conservation of the Chagga homegardens, *Biodivers. Conserv.*, *15*, 1193–1217.
Hemp, A. (2006c), Vegetation of Kilimanjaro: Hidden endemics and missing bamboo, *Afr. J. Ecol.*, *44*, 305–328.
Jin, M., and R. E. Dickinson (2010), Land surface skin temperature climatology: Benefitting from the strengths of satellite observations, *Environ. Res. Lett.*, *5*, 044,004.
Justice, C., J. Townshend, E. Vermote, E. Masuoka, R. Wolfe, N. Saleous, D. Roy, and J. Morisette (2002), An overview of MODIS land data processing and product status, *Remote Sens. Environ.*, *83*, 3–15.
Karl, T. R., R. W. Knight, K. P. Gallo, T. C. Peterson, P. D. Jones, G. Kukla, N. Plummer, V. Razuvayev, J. Lindseay, and R. J. Charlson (1993), A new perspective on recent global warming: Asymmetric trends of daily maximum and minimum temperatures, *Bull. Am. Meteorol. Soc.*, *74*, 1007–1023.
Kastrov, V. G. (1956), Solnechnaia radiatsiia v troposphere v sluvhae absoliutno chistnogo I sukhogo vozdukha, *Trudy Tsentr. Aerol. Obs.*, *16*, 23–30.
Lambrechts, C., B. Woodley, A. Hemp, P. Nnyiti, et al. (2002), Aerial survey of the threats to Mt. Kilimanjaro forests. UNDP, Dar es Salaam.
Lawrimore, J. H., M. J. Menne, B. E. Gleason, C. N. Williams, D. B. Wuertz, R. S. Vose, and J. Rennie (2011), An overview of the Global Historical Climatology Network monthly mean temperature data set, version 3, *J. Geophys. Res.*, *116*, D19121, doi:10.1029/2011JD016187.
Lu, A., S. Kang, Z. Li, and W. Theakstone (2010), Altitude effects of climatic variation on Tibetan Plateau and its vicinities, *J. Earth Sci.*, *21*, 189–198.
Lundquist, J. D., N. C. Pepin, and C. Rochford (2008), Automated algorithm for mapping regions of cold-air pooling in complex terrain, *J. Geophys. Res.*, *113*, D22107, doi:10.1029/2008JD009879.
Maeda, E. E. (2014), Downscaling MODIS LST in the East African mountains using elevation gradient and land-cover information, *Int. J. Rem. Sens.*, *35*(9), 3094–3108.
Maeda, E. E., and P. Hurskainen (2014), Spatiotemporal characterization of land surface temperature in Mount Kilimanjaro using satellite data, *Theor. Appl. Clim.*, doi:10.1007/s00704-013-1082-y.
Maeda, E. E., D. A. Wiberg, and P. K. E. Pellikka (2011), Estimating reference evapotranspiration using remote sensing and empirical models in a region with limited ground data availability in Kenya, *Appl. Geogr.*, *31*, 251–258.
Merchant, C. J., et al. (2013), The surface temperatures of Earth: Steps towards integrated understanding of variability and change, *Geosci. Instrum. Method. Data Syst.*, *2*, 305–321, doi:10.5194/gi-2-305-2013.
Mölg, T., N. J. Cullen, D. R. Hardy, G. Kaser, and L. Klok (2008), Mass balance of a slope glacier on Kilimanjaro and its sensitivity to climate, *Int. J. Climatol.*, *28*, 881–892, doi:10.1002/joc.1589.
Mölg, T., J. H. C. Chiang, A. Gohm, and N. J. Cullen (2009), Temporal precipitation variability versus altitude on a tropical high mountain: Observations and mesoscale atmospheric modeling, *Q. J. R. Meteorol. Soc.*, *135*, 1439–1455.
Mostovoy, G. V., R. King, K. R. Reddy, and V. G. Kakani (2005), Using MODIS LST data for high-resolution estimates of daily air temperature over Mississippi, in *Proceedings of the 3rd International Workshop on the Analysis of Multi-temporal Remote Sensing Images*, 76e80 pp., IEEE.
Nemani, R. R., and J. W. Running (1989), Estimation of regional surface resistance to evapotranspiration from NDVI and thermal-IR AVHRR data, *J. Appl. Meteorol.*, *28*, 276–284.
Ohmura, A. (2012), Enhanced temperature variability in high-altitude climate change, *Theor. Appl. Climatol.*, *110*, 499–508.
Østby, T. I., T. V. Schuler, and S. Westermann (2014), Severe cloud contamination of MODIS land surface temperatures over an Arctic ice cap, Svalbard, *Remote Sens. Environ.*, *142*, 95–102.
Pepin, N., and J. Lundquist (2008), Temperature trends at high elevations: Patterns across the globe, *Geophys. Res. Let.*, *35*, L14701, doi:10.1029/2008GL034026.
Pepin, N., et al. (2015), Elevation dependent warming in mountain regions of the world, *Nat. Clim. Change*, *5*(5), 424–430.
Pepin, N. C., W. J. Duane, and D. R. Hardy (2010), The montane circulation on Kilimanjaro, Tanzania and its relevance for the summit ice fields: Comparison of surface mountain climate with equivalent reanalysis parameters, *Global Planet. Change*, *74*, 61–75.
Qin, J., K. Yang, S. Liang, and X. Guo (2009), The altitudinal dependence of recent rapid warming over the Tibetan Plateau, *Clim. Change*, *97*, 321–327.
Rangwala, I., and J. R. Miller (2012), Climate change in mountains: A review of elevation-dependent warming and its possible causes, *Clim. Change*, *114*, 527–547.
Rangwala, I., J. Miller, and M. Xu (2009), Warming in the Tibetan Plateau: Possible influences of the changes in surface water vapor, *Geophys. Res. Lett.*, *36*, L06703, doi:10.1029/2009GL037245.
Røhr, P. C., and Å. Killingtveit (2003), Rainfall distribution on the slopes of Mt Kilimanjaro, *Hydrol. Sci. J.*, *48*, 65–77.
Schüler, L., A. Hemp, and H. Behling (2014), Relationship between vegetation and modern pollen-rain along an elevational gradient on Kilimanjaro, Tanzania, *Holocene*, *24*(6), 702–713.

Shamir, E., and K. P. Georgakakos (2014), MODIS land surface temperature as an index for surface air temperature for operational snowpack estimation, *Remote Sens. Environ.*, *152*, 83–98.
Shen, S., and G. G. Leptoukh (2011), Estimation of surface air temperature over central and eastern Eurasia from MODIS land surface temperature, *Environ. Res. Lett.*, *6*(4), 045,206.
Shugart, H. H., N. H. F. French, E. S. Kasischke, J. J. Slawski, C. W. Dull, R. A. Shuchman, and J. Mwangi (2001), Detection of vegetation change using reconnaissance imagery, *Global Change Biol.*, *7*, 247–252.
Soini, E. (2005), Land use change patterns and livelihood dynamics on the slopes of Mt. Kilimanjaro, Tanzania, *Agr. Syst.*, *85*, 306–323.
Townshend, J. R. G., and C. O. Justice (1986), Analysis of the dynamics of African vegetation using the normalized difference vegetation index, *Int. J. Remote Sens.*, *8*, 1189–1207.
Urban, M., J. Eberle, C. Hüttich, C. Schmullius, and M. Herold (2013), Comparison of satellite-derived land surface temperature and air temperature from meteorological stations on the Pan-Arctic Scale, *Rem. Sens.*, *5*(5), 2348–2367.
Vancutsem, C., P. Ceccato, T. Dinku, and S. J. Connor (2010), Evaluation of MODIS land surface temperature data to estimate air temperature in different ecosystems over Africa, *Remote Sens. Environ.*, *114*(2), 449e465.
Vuille, M., and R. Bradley (2000), Mean annual temperature trends and their vertical structure in the tropical Andes, *Geophys. Res. Lett.*, *27*, 3885–3888, doi:10.1029/2000GL011871.
Wan, Z. (2006), Collection 5 MODIS land surface temperature products users' guide, ICESS, Univ. of Calif., Santa Barbara.
Wan, Z. (2008), New refinements and validation of the MODIS land surface temperature/emissivity products, *Remote Sens. Environ.*, *112*, 59–74.
Wan, Z., and J. Dozier (1996), A generalized split-window algorithm for retrieving land-surface temperature from space, *IEEE Trans. Geosci. Remote Sens.*, *34*, 892–905.
Wan, Z., Y. Zhang, Q. Zhang, and Z. L. Li (2002), Validation of the land-surface temperature products retrieved from Moderate Resolution Imaging Spectroradiometer data, *Remote Sens. Environ.*, *83*, 163–180.
Wan, Z., Y. Zhang, Q. Zhang, and Z. L. Li (2004), Quality assessment and validation of the global land surface temperature, *Int. J. Remote Sens.*, *25*, 261–274.
Wang, W., S. Liang, and T. Meyers (2008), Validating MODIS land surface temperature products using long-term nighttime ground measurements, *Remote Sens. Environ.*, *112*, 623–635.
Wenbin, Z., L. Aifeng, and J. Shaofeng (2013), Estimation of daily maximum and minimum air temperature using MODIS land surface temperature products, *Remote Sens. Environ.*, *130*, 62–73.
Westermann, S., M. Langer, and J. Boike (2012), Systematic bias of average winter-time land surface temperatures inferred from MODIS at a site on Svalbard, Norway, *Remote Sens. Environ.*, *118*, 162–167.
Whiteman, C. D., J. M. Hubbe, and W. J. Shaw (2000), Evaluation of an inexpensive temperature datalogger for meteorological applications, *J. Atmos. Oceanic Technol.*, *17*(1), 77–81.
Yan, L., and X. Liu (2014), Has climatic warming over the Tibetan Plateau paused or continued in recent years?, *J. Earth Ocean Atmos. Sci.*, *1*, 13–28.
You, Q., S. Kang, N. Pepin, W.-A. Fluegel, Y. Yan, H. Behrawan, and J. Huang (2010), Relationship between temperature trend magnitude, elevation and mean temperature in the Tibetan Plateau from homogenized surface stations and reanalysis data, *Global Planet. Change*, *71*, 124–133.